MyrrhaFoam: A CFD model for the study of the thermal hydraulic behavior of MYRRHA

Lilla Koloszar and Sophia Buckingham [*]
Von Karman Institute for Fluid Dynamics
B-1640, Rhode-St-Genese, Belgium
lilla.koloszar@vki.ac.be ; sophia.buckingham@vki.ac.be

Steven Keijers
SCK.CEN
B-2400 Mol, Belgium
skeijers@sckcen.be

ABSTRACT

Numerical analysis of the thermohydraulic behavior of the innovative flexible fast spectrum research reactor, MYRRHA, under design by the Belgian Nuclear Research center (SCK•CEN) is a very challenging task. The primary coolant of the reactor is Lead Bismuth Eutectic, LBE, which is an opaque heavy liquid metal with low Prandtl number. The simulation tool needs to involve many complex physical phenomena to be able to predict accurately the flow and thermal field in the pool type reactor.

In the past few years, within the frame of a collaboration between SCK•CEN and the von Karman Institute, a new platform, MyrrhaFoam, was developed based on the open source simulation environment, OpenFOAM. The current tool can deal with incompressible buoyancy corrected steady/unsteady single phase flows. It takes into account conjugate heat transfer in the solid parts which is mandatory due to the expected high temperature gradients between the different parts of the reactor. The temperature dependent properties of LBE are also considered. MyrrhaFoam is supplemented with the most relevant thermal turbulence models for low Prandtl number liquids up to date.

KEYWORDS
computational fluid dynamics, heat transfer, , liquid metals, fast reactors

1. INTRODUCTION

The Belgian Nuclear Research Centre is working since several years on the design of MYRRHA, a flexible fast spectrum nuclear reactor. This is a global first demonstration project for a new type of reactor, piloted by a particle accelerator – ADS. The thermal hydraulics of nuclear applications imposes huge challenges to numerical solvers due to the wide range of scales and physics involved in such flows. Industrial approaches are necessary to support the design phase of new nuclear reactors and to analyze already existing ones. This work shows the numerical development of a simulation environment that can handle all the relevant physical aspects from thermal hydraulic point of view.

During the design phase of the MYRRHA reactor, the geometry is constantly evolving. The current study is based on version 1.4. A picture of the reactor and the relevant physical aspects is proposed in Figure 1. The numerical simulation aims to resolve the primary coolant flow and heat transfer. Conjugate heat transfer plays a significant role due to the high gradients, so its effect is considered, as well. The primary

coolant of the reactor is Lead Bismuth Eutectic, a heavy liquid metal with low Prandtl number. Its material properties are highly dependent on temperature; known correlations could be taken from the LBE Handbook [1]. Above the LBE in the reactor Argon gas is placed and free surfaces are formed. The need to represent the free surface in the simulations depends on the operating conditions investigated.
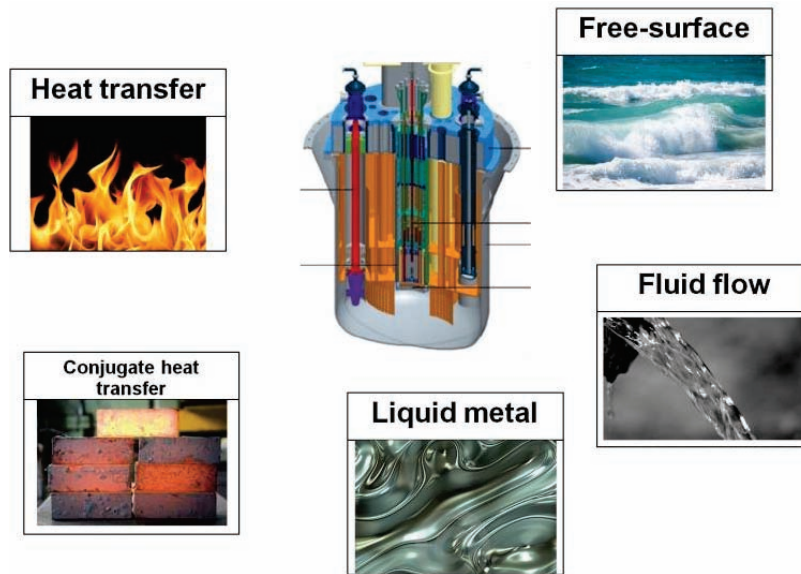
Figure 1: The MYRRHA reactor and physical considerations

In this paper the reactor in nominal operation is considered. Since the level of the free surfaces are constant in this scenario, the resolution of the free surface is not strictly needed, so two approaches were taken: a single phase simulation was performed to get insight to the flow and thermal fields of the reactor, then a multiphase solution was considered to initialize later transient simulations with changing positions of the free surface levels, such as primary pump start up and shut down or accident scenarios e.g. primary pump failure. First the development steps of the physical and modeling aspects will be introduced then the nominal flow simulation of single and multiphase flows will be described and compared. Finally conclusions and further work perspectives will be given.

2. PROBLEM DRIVEN SOLVER DEVELOPMENT

The flow and thermal field in the reactor is very complicated, coupled with a complex geometry. Therefore, an incremental approach was considered in the solver development. Every step was verified by results obtained with a reference solution. In general, some processes in the reactor are not relevant from the thermal hydraulics of the primary cooling aspects, such the nuclear reaction in the core, so only there effects on the Lead Bismuth Eutectic flow is taken into account. In the following, the numerical domain for the nominal operation will be shown with the introduction of the basic modeling approaches.
Material properties
The temperature dependent thermal properties of the LBE have been taken from the LBE handbook [1]. Linear or second order interpolation of experimental data collected in the database for molten LBE yields for the LBE density ρ_{LBE}, conductivity λ_{LBE} and heat capacity $C_{P_{LBE}}$:

$$\rho_{LBE} = 11096 - 1.3236T \tag{1}$$
$$\lambda_{LBE} = 3.61 + 1.517 \times 10^{-2}T - 1.741 \times 10^{-6}T^2 \tag{2}$$
$$C_{P_{LBE}} = 159 - 2.72 \times 10^{-2}T + 7.12 \times 10^{-6}T^2 \tag{3}$$

where temperature T is in Kelvin. As for dynamic viscosity μ_{LBE}, the viscosity database yields the following correlation:

$$\mu_{LBE} = 4.94 \times 10^{-4} e^{754.1/T} \tag{4}$$

These relationships had to be implemented in OpenFOAM, where a new, temperature dependent material class has been introduced to be able to model any fluid with quadratic temperature dependent specific heat and density and exponential viscosity such as LBE. The solid regions are defined as AISI 316L steel. Thermal properties are found in the Atlas technical handbook [9], where:

$$\rho = 8000 \text{ kg. m}^{-3}, \quad \lambda = 11.45 + 0.013T, \quad C_p = 500 \text{ J. K}^{-1}. \text{kg}^{-1} \tag{5}$$

During the design phase of the MYRRHA reactor, the geometry is constantly evolving. It was decided to perform the study based on version 1.4 of the reactor. A picture of the CAD used for the CFD simulations is shown in Figure 2.

Approach for pump simulation
The flow field within the reactor is driven by the pumping system. There are two HX/Pump casing, each one consisting of two HX and one pump. In the global CFD loop, these casings had to be considerably simplified to limit the complexity of the model. Concerning the pumps, modeling the flow through the rotor would require meshing around the blades and modeling the dynamic behavior of these rotating parts. This level of refinement is not required since we are only interested in respecting the nominal flow conditions of the primary coolant loop. The presence of the rotor was therefore neglected in the CFD model shown in Figure 2.
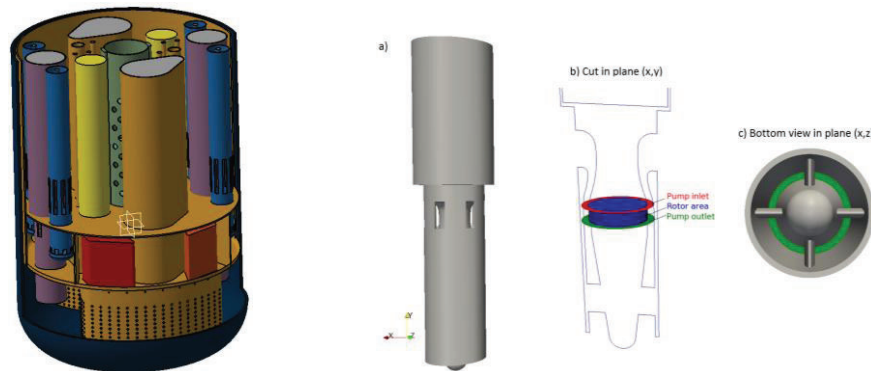
Figure 2: The numerical model of the MYRRHA reactor and the pumps: solid pump component, rotor area and pump inlet/outlet surfaces and bottom view

There are two possible ways of representing the pumps: by either having an open or a closed system. In the first case, the rotor area (annular volume between red and green ring) is removed from the CFD domain and the nominal mass flow rate is imposed at the pump's outlet (green surface), by specifying velocity conditions. The mass flow rate is an important parameter of the MYRRHA reactor and has been fixed to 9440. kg/s under nominal conditions. Reference pressure is then given at the pump's inlet (red surface). However, in case of transient simulations such as pump failure for instance, a closed-loop is needed. Flow motion is then activated by a momentum source applied to the rotor area, and fixed to balance the desired mass flow rate. In the current work, the first approach is followed, the pump is represented by an inlet and an outlet region and an open loop is considered.
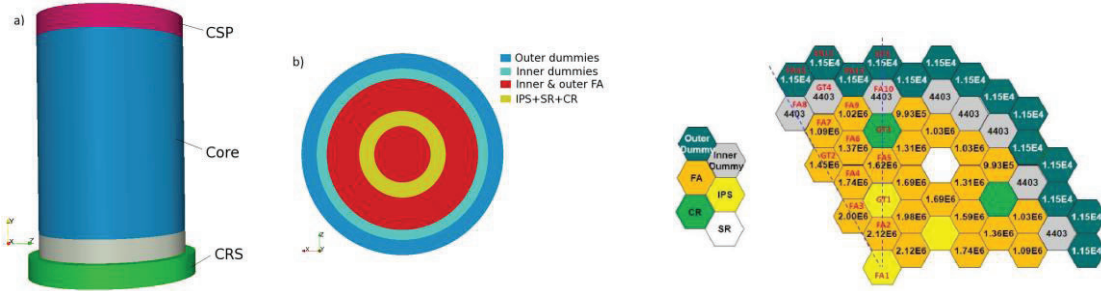
Figure 3: The a) General porous media in the central part of the reactor b) Core layout decomposition c) radial power distribution in the MYRRHA reactor core

The core has been modeled following the homogenization approach with porous modeling. The different zones are separated according to the structures layout, which is governing both porosity and pressure losses. Consequently, the general core layout, shown in Figure 3, is composed in the central core of 5 porous rings of 1.78 m high, representing from the centre: the inner FA, the combination of IPS+SR+CR, the outer FA, the inner dummies and the outer dummies. The last ring corresponding to the core jacket is a solid component and was therefore subtracted from the flow domain. The area directly below the core, composed of a grid with cones that hold the FA in place, makes the connection with the core restraint system, CRS. As this intermediate ring is characterized by very little flow blockage from either axial or radial directions, it is approximated as a non-porous zone.

However, it should be noted that in reality the IPS, SR and CR are arranged separately between the FA, thus approximating this area to a single ring is a non-negligible assumption in terms of momentum and heat transfer. Each of these porous zones is characterized by a certain porosity value γ, defined as the ratio between the volume of fluid and the total volume of the media. From a numerical point of view, these pressure losses due to friction are added to the standard equation as a momentum sink expressed as follows:

$$\vec{F_i} = -\frac{\mu}{\alpha}\vec{u_i} - \frac{\rho}{2}C_2|\vec{u}|\vec{u_i} = \nabla p_{porous} \tag{6}$$

In this application, due to the low velocities and the low viscosity of the LBE, the viscous losses are neglected such that only the second term representing inertial resistance is considered. The second parameter to specify is the inertial resistance coefficient C_2 in each direction. Therefore, once the expected pressure drop Δp_{porous} along the reference length L_{ref} is known, C_2 can be estimated according to the estimated flow rate as follows:

$$C_2 = \frac{\Delta p_{porous}}{L_{ref}\frac{\rho}{2}\tilde{u}^2} \tag{7}$$

It is important to note that it is the superficial velocity $\tilde{u}$ that needs to be considered in the above equation, equal to the equivalent velocity in a fully open media. It is calculated by multiplying the real velocity by the media's porosity. Consequently, each porous media is defined by a porosity γ value and an inertial resistance coefficient $(C_{2,r}, C_{2,y})$ in the radial and axial direction respectively. As the parallel channels connect the lower plenum with the upper plenum, the mass flow rate distribution is a result of the different porosities. The pressure drop across the entire core area, from the lower plenum up to the free-surface (including the radial losses through the barrel holes) is estimated to about 2 bars. Due to hexagonal wrapper tubes of the fuel assemblies in reality the flow is blocked in the radial direction in the porous media. This condition is imposed numerically by assigning a very high value to $C_{2,r}$ (1000 /m) in

the core region. The cross sections of the rings are determined with respect to the fractions of core positions taken. In critical configuration, the core of MYRRHA is made up of 69 fuel assemblies, 24 inner dummies, 42 outer dummies, 3 SR, 6 CR and 7 IPS . The desired mass flow rate distribution for this simplified model is based on the cross sectional areas and the nominal total mass flow rate of 9440. kg/s. The mass flow distribution can be found in Table I.

Table I. Sample Theoretical mass flow distribution

Core rings	Theoretical distribution
FA	5186
IPS+SR+CR	350
Inner dummies	1804
Outer dummies	2100
Total	9440

The pressure drop in normal operation is determined by the pressure drop in the FA. These losses are estimated by using the Rehme correlation for a wire wrapped fuel bundle as a function of the local Reynolds number (noted as f(Re)):

$$\Delta P = f \frac{L_{pin}}{D_{eq}} 0.5 \rho u^2 \tag{8}$$

In the above equation, u is the local flow velocity, L_{pin} corresponds to the pin length, D_{eq} is the equivalent diameter and f is the friction factor given by:

$$f = \left(\frac{64}{Re} F^{0.5} + \frac{0.0816}{Re^{0.133}} F^{0.9335} \right) N_r \pi (D_r + D_w) \frac{1}{St} \tag{9}$$

where N_r is equal to the number of pins, D_r is the clad outside diameter and D_w is the wire diameter. The geometrical factor F is fixed to 1.225. More details are available in [2]. The formulas given by equations (4) and (5) are implemented within the numerical model by defining a new porous model class, using local velocity to calculated Re and f. This dependency is denoted as f(Re) in Table II. The inner dummies are modeled as the FA rings since these have the same flow rate and pressure drop. The axial resistance coefficient of the two other core rings, IPS+SR+CR and outer dummies, was kept constant and first approximated based on the desired mass flow rate distribution, from which an average LBE velocity can be extracted. The values were then slightly adjusted to get closer to this distribution. The final porous media parameters are summarized in Table II. For the core support plate, CSP and the CRS regions, their axial resistance coefficient was calculated to reach a total pressure drop of 2 bars across the whole central region of the reactor.

Table II. Porous material setup in the core

Porous zone	Porosity: γ	Axial resistance $C_{2,y}$ (/m)
CSP	0.15	24
Core inner FA	0.44	f(Re)
Core IPS+SR+CR	0.15	374
Core outer FA	0.44	f(Re)
Core inner dummies	0.44	f(Re)
Core outer dummies	0.28	74
CRS	0.15	67

The heat in the core is modeled as a volumetric heat source of 100 MW in total and is limited to the inner and outer FA rings, where the nuclear reaction is significant. The foreseen radial power distribution is approximated by a third order polynomial to approach an integrated power of 24.6 MW and 75.4 MW in

the inner and outer FA rings. A detailed description of the real and fitted distributions is given in Figure 4/a. As can be seen, the functional source is only active where the fuel elements are placed in the core. In order to apply to heat distribution and the previously described momentum terms the *expressionSource* functionality of the swak4foam toolbox is linked to the myrrhaFoam solver. By this way, through a control file any kind of analytical function can be prescribed by the user.
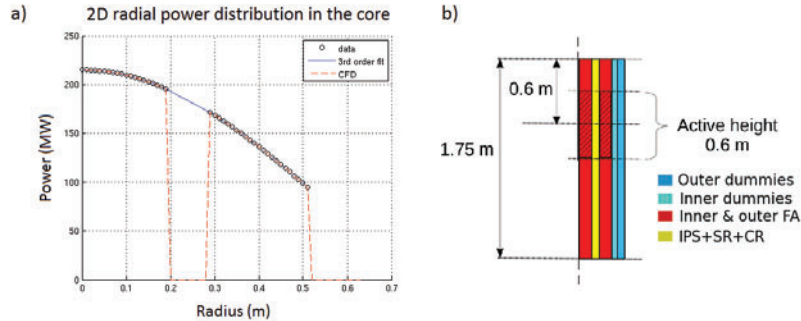
Figure 4: a) Radial heat source distribution b) Axial positioning of the heat source

In the axial direction, the shape is a cosine profile of half a period, reaching a maximum in the active core centre represented in hatching on Figure 4/b. However, the cosine reaches only zero at 1.035 m and power is limited to this active height of 0.6 m. The final expression used to model the core heat source distribution is the following, given in W/m3:

$$Q_{core}(r, y) = Q_0 \cos\left[\frac{\pi}{h}(y + h_0)\right] f(r))$$ (10)

Where h is the active fuel length, h_0 is the projected initial of the cosine fitting.

Barrel and above core structure simulation
The barrel is an integral part of the core support structure, CSS, and is located in the centre of the reactor. It guides the LBE flow from the outlet of the core to the upper (hot) plenum HP through 11 rows of ten 200 mm holes. The barrel surrounds the above core structure,ACS that contains a number of guide tubes and instrumentation tubes. The holes insure the mixing of the LBE as it passes from the core into the HP. However, the original CAD has been modified for the single phase simulation to match the numerical domain where the LBE is present, delimited by the free-surface level, positioned in the middle of the 7th row of barrel holes (starting from the bottom). Therefore, the geometry was cut at exactly this level, omitting the upper part, as shown in Figure 5 a).
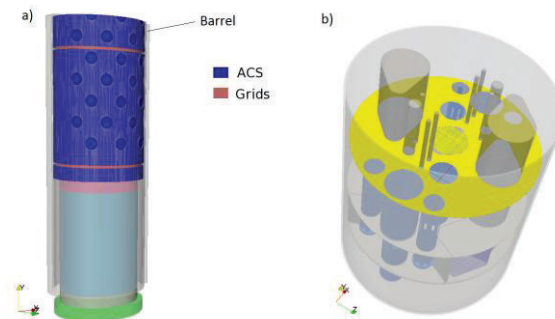
Figure 5: a) Porous media representation of the ACS b) Hot plenum and barrel free-surfaces

Once again the porous media approach is used to model the region inside the barrel. At intermediate positions along the ACS, two grids guide the IPS, CR and SR tubes into the core. These are modeled as

separate porous zones through which the axial pressure drop is estimated. However, from the free level of LBE to just above the outlet nozzles of the fuel assemblies, the ACS is a much more open structure, also modeled as a porous media. Derivation of porous media properties of the ACS were based on the book: Nuclear Systems by Todreas and Kazimi [3]. By taking into account the presence of all guiding tubes, a porosity of 0.91 is calculated. All porous media parameters are summarized in Table III. The LBE free-surface of the HP is highlighted in yellow in Figure 5 b). As introduced previously, in the single phase full power simulation the free surfaces are approximated by a free slip condition since their level is not expected to vary much at steady state. In addition, the hot plenum (HP) and barrel region free-surface levels are approximated to be at the same height, although a slight difference exists in reality.

Porous media approach in the primary heat exchangers
After having collected the heat from the nuclear reaction, the hot LBE in the HP is aspirated by the pumps into the four heat exchangers. There, the heat is transferred to the secondary coolant which is a mixture of liquid and steam water like in most nuclear power plants. The type of heat exchanger is a counter-current flow heat exchanger with straight tubes. The HX design is shown in Figure 6 a). The LBE is flowing outside the water tubes downwards, while the two-phase water is flowing upwards. In normal operation, the HX's have to remove the power generated by the reactor core and all of the other heat sources (e.g.spent fuel, pumps). Therefore, it was designed to extract 110 % of the nominal core power to take all of these into account. The number and dimensions of the water tubes should therefore be sufficient for the HX to extract 27.5 MW. Each HX consists of 684 water tubes with an external diameter of 16 mm. In the CFD model however, the HX is simplified using the porous media approach which avoids having to represent the hundreds of water tubes. Only the feed water pipe in the centre is represented and subtracted from the numerical domain as the secondary circuit is not modeled. Based on the cross-sectional area occupied by water tubes, the porosity is calculated. As previously, the theoretical average velocity allows us to estimate the pressure losses which in turn provide us with the inertial resistance coefficients. All values are summarized in Table III. As observed in Figure 6 b), the porous media (in blue) occupies all of the interior volume of the HX, except the feed water line, which is taken into account as solid surface (in red). Also here the simulation domain is limited by the height of the LBE free-surface level.

Table III. Porous material setup in the heat exchanger and above the core

Porous zone	Porosity: γ	Axial resistance $C_{2,y}$ (/m)	Radial resistance $C_{2,r}$ (/m)
ACS	0.91	0	4
Grids	0.85	2	1000
HX	0.62	1.55	32

The heat transfer between the primary and secondary coolant is represented in the CFD model by a variable heat sink located in the HX porous zone. The heat transfer correlation derived by Ushakov [4] for liquid metal and recommended for rod bundles in a triangular or hexagonal arrangement is used. The following expression for the Nusselt number Nu is applied:

$$Nu = 7.55\frac{P}{D} - 20\left(\frac{P}{D}\right)^{-3} + \frac{3.67}{90(P/D)^2}Pe^{\left(0.19\frac{P}{D}+0.56\right)} \tag{11}$$

As described by equation (12), the heat transfer that occurs at the water tube boundary will depend on the pitch to diameter ratio P/D and the Peclet number Pe. The latter is related to the Reynolds number Re and the Prandtl number Pr, such that:

$$Pe = Re.Pr, \text{ with: } Re = \frac{\rho u_{magn} D_H}{\mu} \quad \& \quad Pr = \frac{\mu C_P}{\lambda} \tag{12}$$

In the simulation, the local velocity magnitude u_{magn} is considered to calculate the local heat transfer described by Nu. The latter is then used to determine the heat transfer coefficient h_e on the LBE side, given by:

$$h_e = \frac{Nu.\lambda}{D_H} \tag{13}$$

Finally, the total local heat transfer U is determined, considering also the water tube's heat transfer resistance R and the heat transfer coefficient h_i on the water side, as follows:

$$U = 1 / \left(\frac{1}{h_e} + R + \frac{1}{h_i} \right) \tag{14}$$

As for the core, the heat sink S_{PHX} is volumetric, therefore it takes into account the water tubes' exchange surface $A_{exchange}$, the HX's volume V_{HX} and the local temperature difference between the LBE and the water, such that:

$$S_{HX} = UA_{exchange}(T - T_{water})/V_{HX} \times F_{HX} \tag{15}$$
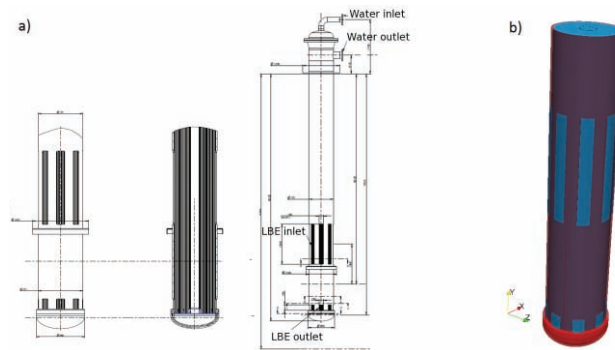
Figure 6: a) HX design b) HX with porous media modeling

The water temperature T_{water} is fixed to 200 °C. An additional factor F_{HX} appears in order to adjust the heat that is removed. The factor F_{HX} was fixed to 0.52 so that approximately 25.5 MW would be removed by each HX when heat losses are neglected.

IVFS simulation
The IVFS (In Vessel Fuel Storage) consists in four racks, each capable of storing half a core, with 76 positions where the FA can be placed. Instead of representing individually the different positions, this component is simplified using a porous media that surrounds all the storing positions. This region is defined by considering that the racks are fully occupied by the FA. Consequently, the same parameters are taken for the IVFS porous media than for the FA rings. Finally, in terms of heat modeling the IVFS represent an additional source of energy since the stored FA release some residual heat. Thus, a uniform heat source is added in each of them so that an extra 2 MW is injected in total. It is important to mention that LBE is able to flow within the IVFS to help cool down the FA by natural convection. To allow the coolant circulation, several holes are placed in the cylindrical shell of the inner vessel between the two plates of the IVFS casing.

3. ANALYSIS OF THE NOMINAL OPERATION OF THE MYRRHA REACTOR IN SINGLE PHASE FLOW ENVIRONMENT

Finite Volume codes are more accurate with hexahedral meshes, as the flow is better aligned with the grid. In order to obtain a hexahedral based mesh for the reactor simulations, the mesh generator included in the OpenFOAM package, called snappyHexMesh was used [6]. The snappyHexMesh utility generates 3-dimensional meshes containing hexahedra (hex) and split-hexahedra (split-hex) automatically from triangulated surface geometries in Stereolithography (STL) format. The mesh approximately conforms to the surface by iteratively refining a starting mesh and morphing the resulting split-hex mesh to the surface. The specification of mesh refinement level is very flexible and the surface handling is robust with a pre-specified final mesh quality. The mesh generator is script driven and completely automatic. Geometry modifications therefore can be taken into account easily. It runs in parallel with a load balancing step at each iteration, which makes it very efficient.

First a basic background mesh was generated with a global mesh size of 30cm. This basic mesh is then refined 4 times around the surfaces and edges to get a good representation of the geometry with a refinement ratio 1:2 (cell volumetric ratio between coarse and fine section). Three different refinement regions were defined in order to capture the pump jets and the jet below the core. Finally, the refined mesh is snapped to the surfaces to capture the geometric complexity correctly. In order to represent the shear stress on the walls without resolving fully the boundary layers, wall functions has been used. The corresponding average y^+ of the mesh is around 400, with a minimum of 120 and maximum of 1200. The fluid and the solid mesh is generated together resulting in a fully conformal mesh between the fluid and the solid regions. In addition to the inner vessel, the other major solid parts are meshed so that CHT can also be simulated through these structures. The solids located in between LBE regions of high temperature gradients appear to be the walls of the in vessel fuel handling machine, IVFHM and the two diaphragm plates. In the CAD created for the CFD model, together with various tubes these two components are included within a single part referred to as main-walls and colored in grey in Figure 7 a). Therefore, all of these components are meshed at once as a single solid domain (grey domain). In addition, the blue region representative of the closed LBE zone surrounding the core is also meshed. The last solid parts added to the simulation are all four HX walls, as shown in Figure 7 b) with a picture of one of the meshes.
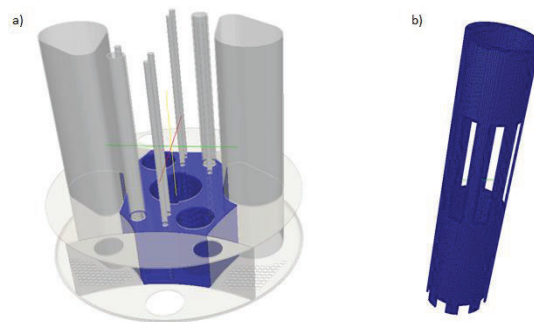
Figure 7: a) 'Main-walls' component in grey and closed LBE region in blue b) Mesh of the solid HX

The steady state solver developed within this work is solving the Reynolds-Averaged Navier-Stokes equations (RANS) with temperature as a passive scalar in the single phase environment. The pressure and velocity field is coupled through the SIMPLE algorithm. The momentum and turbulent models are extended to buoyant flows. In the current simulation the standard k-ε model was used. To predict the effect on turbulence heat transfer the Reynolds analogy was considered with a constant turbulent Prandtl number equal to 2.8 as suggested by [10] for LBE. Conjugate heat transfer is taken into account through

defining solid and fluid regions. Inside these regions, different equations are solved, RANS for the fluid and only heat transfer in the solid. The coupling between the two regions is done through boundary conditions, which ensures the same velocity of the wall from the solid and the fluid side and the same heat flux. The resulting linear equations are solved by a V-cycle type Algebraic Multigrid method. Due to the high power of the core, large gradients of temperature are expected in the reactor. In order to resolve the heat transfer across the solid walls, conjugate heat transfer was used. As mentioned previously, the free surfaces are modelled as zero shear slip walls in the single phase setup. This implies mirror symmetry of the flow/thermal solution and therefore a symmetry boundary condition is applied. We also recall that an inlet mass flow rate of 9440. kg/s is imposed at the pump's outlet for the single phase simulation. The turbulent kinetic energy k at this   plane is calculated as:

$$k_{in} = \frac{1}{2}\left(u'^2_x + u'^2_y + u'^2_z\right) = \frac{1}{2}\left[u'^2_x + 2\left(\frac{1}{3}u'_x\right)^2\right] = \frac{11}{18}(I_u.U_x)^2 \tag{16}$$

Assuming a turbulence intensity level I_u of 10 % and a velocity of 2.45 m/s extracted from a preliminary calculation, this yields: $k_{in} = 0.15$ m². s^{-2}. Turbulent dissipation ε is given by the following expression:

$$\varepsilon_{in} = \frac{C_\mu^{0.75}.k_{in}^{1.5}}{l} \tag{17}$$

where the coefficient C_μ is equal to 0.09. Considering essentially main flow in this region, it is common to approximate the turbulent length scale l as 7 % of the hydraulic diameter D_H, such that: $\varepsilon_{in} = 1.3637$ m². s^{-3}. Finally, an outlet pressure equal to the operating pressure of 0 Pa is applied to the pump's inlet for the steady state simulation.

The first objective of the full power simulation is to get an insight into the large flow patterns that develop within the reactor. These are essential to get a general understanding of the flow field and identify possible areas where low LBE refresh rates may occur. Indeed, such stagnant zones need to be avoided since oxygen control has to be kept within narrow limits. The second objective of this simulation is to evaluate the temperature distribution on the different components for stress evaluations.
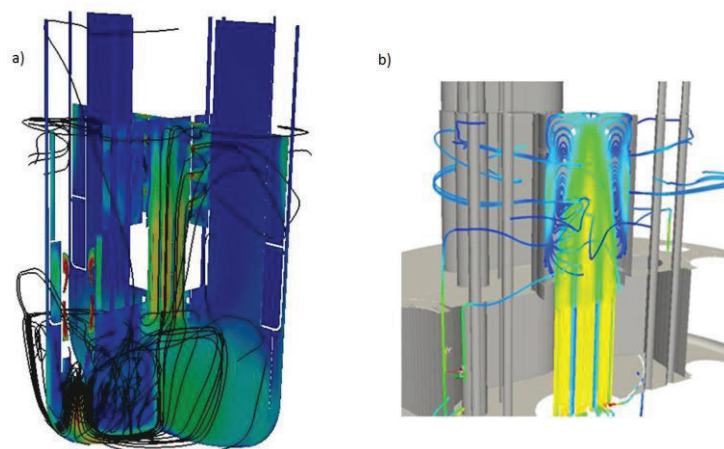
Figure 8: a) Velocity contours and streamlines in the vertical symmetry planes b) Streamlines in the barrel region

The overall pressure drop through the primary coolant loop is 2.57 bars. One of the most important parameters of the reactor is the pressure drop through the core. We recall that a pressure drop of 1.7 bars

is expected in the core region while about 2 bars should be obtained between the CP and HP respectively. The resulting values from the simulation indicate very small differences of less than 2 % in both the core and between the CP and HP. The maximum pressure difference on both the barrel and HP free-surfaces is at most 1.5 kPa. This would be equivalent to a height variation of 1.5 cm, therefore underlying the practically flat aspect of these surfaces. This confirms that modeling the free-surfaces as a zero-shear slip wall is acceptable for this operational condition.

A general description of the flow field can now be proposed based on the flow streamlines shown in Figure 8. The two pump jets first impact the bottom of the vessel before merging in the centre of the lower plenum leading to an upward flow directed towards the core. The flow is distributed as expected through the different core rings. Within the above core structures a central upward plume is formed going until the free surface level. Once the flow reaches the free-surface, part of it exits through the last row of barrel holes but a large portion goes back down into the barrel before exiting through the other rows of holes lower down. Finally, the flow in the upper plenum goes back into the HX. Contours of velocity are given in Figure 9 in the two vertical symmetry planes (indicated on the top view), with levels between 0-1 m/s and saturated above. The nominal mass flow rate leads to a maximum velocity of 2.37 m/s in the pumps.
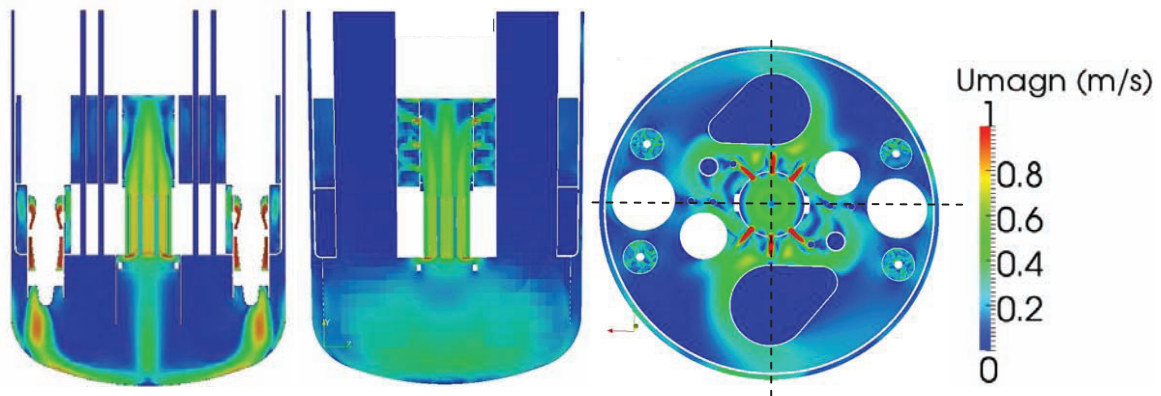
Figure 9: Velocity magnitude contours in the vertical symmetry plane z=0

As for the flow in the symmetry plane cutting the barrel holes, long vertical jets originating from the different core rings appear in the ACS. Unlike in the perpendicular plane, mixing is limited and the LBE exits progressively through the barrel holes. The jets from the holes facing the IVFHM collide with the chimney structures.

Verification of the porous core approach
One of the important modelling requirements to fulfill is to approach the desired mass flow rate distribution in between the different core rings. A good agreement is obtained with the proposed porosity and resistance settings in the porous media of the core. The relative differences compared to the desired flow rates stay below 5%. These differences remain acceptable and no further adjustment is required.

The various heat sources and sinks used for thermal modelling result in substantial temperature variations throughout the reactor. We recall that 100 MW is injected across the core and an additional 2 MW are added in total in the IVFS, where the used FA are stored. In steady state this same amount of heat (102 MW) is extracted by the four HX since thermal losses to the exterior are neglected for the moment. The water side temperature of the HX of 200°C act as fixed reference temperature. The turbulent Prandtl number was fixed to 2.8 according to the literature in the following study [7,8]. Static temperature contours in the vertical symmetry planes are shown in Figure 10. One can see that due to mixing, the core

heat source located in the inner and outer FA rings heats up the flow coming out from the other rings as the flow rises. A maximum temperature of 471 °C is reached in the core. The mass flow average core inlet and outlet temperatures correspond to 272 °C and 344.5 °C respectively, in agreement with an injected power of 100 MW $\left(P = \dot{m}C_p\Delta T\right)$.
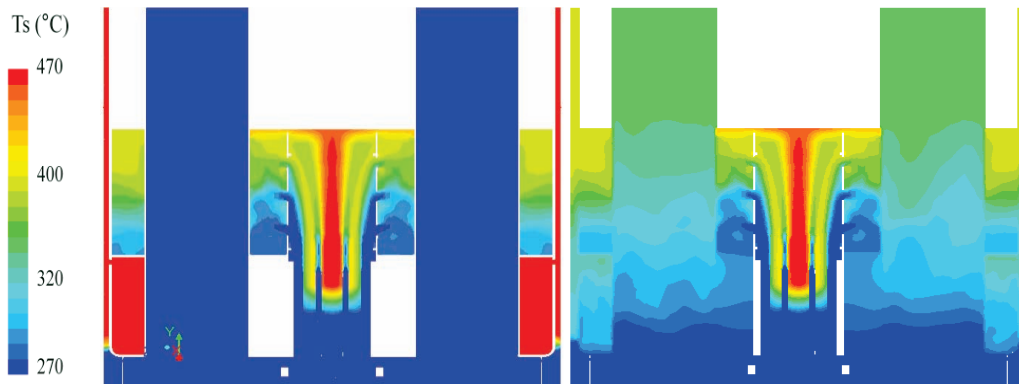
Figure 10: Effect of conjugate heat transfer (left without, right with CHT)

Figure 10 shows clearly the importance of the CHT. By the conduction through the structures the temperature differences between the cold and hot plenum in the upper region of the reactor (annular space and IVFHM) are smoothened. As illustrated in Figure 10, LBE is being ejected through the barrel holes at different temperatures. Considering the lack of flow mixing in this plane, the cold flow from the outside rings tends to exit through the first rows of holes while the central hot jet in the core reaches the free-surface. Average temperatures on the barrel and HP free-surfaces are approximately equal to 440 °C and 400 °C respectively. In the HP, buoyancy prevails and results in a thermal stratification, as shown in Figure 11, where vertical temperature variation in the HP is plotted along a vertical line (Figure 11).
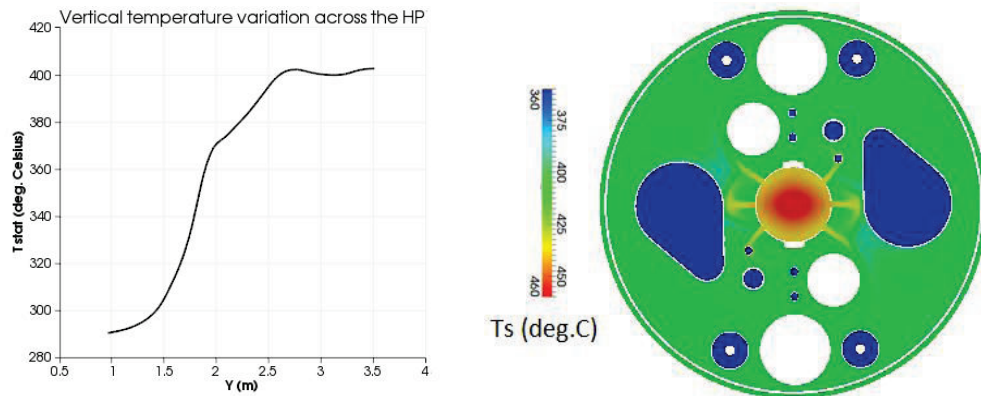
Figure 11: Thermal stratification along a vertical line in the HP indicate position on figure and Static temperature contours on the free-stream surface

To assess the thermal stresses experienced by the various components of the reactor, static temperature contours on either side of the parts are shown in Figure 12. In the simulation without CHT, the internal structures experience temperature gradients by being in contact with the LBE in the two parts of the pool (HP & CP). A maximum temperature difference across the wall of around 60 °C appears at the upper diaphragm plate, where the HX outlet region (270 °C) is located on the lower side and the hot flow (~320 °C) in the HP located on the upper side. Temperatures on the diaphragm and in particular its two horizontal plates are shown in Figure 12/b. As for the top plate, strong gradients exist across its surface

but the differences on either side, of importance for thermal stresses, are limited to similar levels than for the bottom plate.

In the simulations with CHT where the conduction through these plates cools down the hot LBE located in the IVFS area the temperature gradient between this zone and the CP is considerably reduced, which reduces thermal stresses on the lower diaphragm plate (< 30 °C).
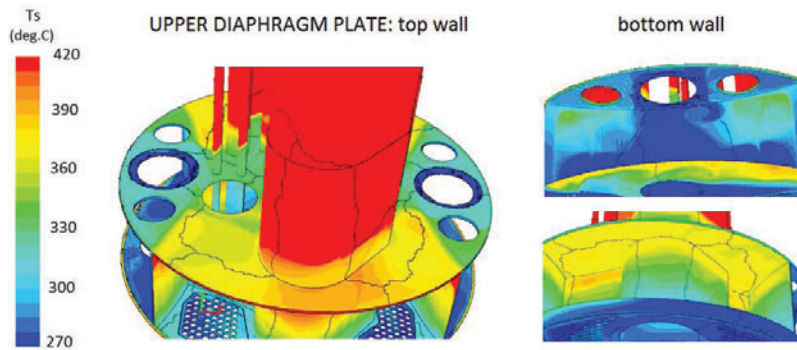
Figure 12: Static temperature contours on the top and bottom sides of the diaphragm plates

4. CONCLUSIONS

Due to the complex geometry and the interaction of the various physical phenomena in a nuclear reactor, the numerical analysis of such systems is very challenging. In this paper the first stage of the development of a numerical solver is presented that can deal with the relevant physics needed to predict the flow and the thermal field of the primary coolant loop of the MYRRHA nuclear reactor. The MyrrhaFoam solver is able to handle temperature dependent material properties, porosity fields with pressure drops according to the Rheme correlation, capable of computing heat transfer in the flow and conjugate heat transfer in the solid parts.

All these developments made it possible to construct a numerical model for the nominal operation of the MYRRHA reactor and analyze the fluid and thermal field of the primary coolant loop. In order to be able to handle the complex geometry of the reactor, several geometrical simplifications have been introduced, and the porous material concept applied to retain the effect of these complex sections. The nominal mass flow is imposed at the pump section and the expected pressure and mass-flow distribution is achieved by setting the porous regions accordingly.

Once the general flow field was established according to the expected mass flow distribution in the core, the thermal sources were activated and after a long transient the thermal filed was analyzed. In the hot plenum, due to the high temperature differences in the stratified flow the structural part are exposed to high thermal stresses. The described steady state simulation can only give an overall average thermal stress field, leading to the possibility of analyze static load on the structures. Though steady RANS simulations can give the r.m.s. fluctuating thermal field, using it for design data is questionable, especially since the applied Reynolds analogy for the thermal turbulence modeling is uncertain for low Prandtl fluids. Thus, in the future the effect of thermal turbulence modeling will be investigated to improve the reliability of the myrrhaFoam solver. Moreover, an unsteady, two phase solver is under development to be able to continue the analysis of the MYRRHA reactor outside of nominal operating condition.

REFERENCES

1. *Handbook on Lead-bismuth Eutectic Alloy and Lead Properties*, Materials Compatibility, Thermal-hydraulics and Technologies, Nuclear Energy Agency 2007 Edition http://www.nea.fr/html/science/reports/2007/nea6195-handbook.html
2. R. Rehme, "Pressure drop and velocity distribution in rod bundles with spacer grids" *Nuclear Engineering and Design*, **Volume 62**, Issues 1-3, page 349-359 - December 1980.
3. R. Rehme, "Pressure drop correlations for fuel elements spacers", *Nuclear Technology*, **Volume 17**, page 15-23, 1973.
4. N. E. Todreas and M. Kazimi: *Nuclear Systems I-II.,* 1990.
5. P. A. Ushakov, "Problems of Heat Transfer in Cores of Fast Breeder Reactor, Heat Transfer and Hydrodynamics of Single-phase Flow in Rod Bundles", *Izd. Nauka*, Leningrad (Russia), 1979.
6. http://www.openfoam.org/docs/user/snappyHexMesh.php
7. A. Borgohain, N. K. Maheshwari, P.K. Vijayan and R. K. Sinha, "CFD analysis on heat transfer in low Prandtl number fluid flows", NURETH14-457, September 2011.
8. A.J. Reynolds, "The prediction of turbulent Prandtl and Schmidt number", International Journal of Heat Transfer, **Volume 18**, pp. 1055-1069, 1975.
9. http://www. atlassteels.co.nz/site/pages/technical-handbooks-of-stainless-steel.php
10. Duponcheel, M. Bricteux, L. Manconi, M. Winckelmans, G. Bartosiewicz, Y., "Assessment of RANS and improved near-wall modeling for forced convection at low Prandtl numbers based on les up to Reτ = 2000", *International Journal of Heat and Mass Transfer,* **Volume 75,** 2014